1 Definition of terms and calculation procedures

1.1 HTDMA errors

The hygroscopic growth factor probability distribution $p(GF)$ was corrected for small deviations (typically $\pm 2\% \text{RH}$) from the setpoint RH, as outlined by Gysel et al. (2009) and calculated as follows:

$$\overline{GF}_{D_0,RH,c} = \left(1 + (\overline{GF}^3_{D_0,RH_m} - 1)\frac{(1 - RH_m)RH_t}{(1 - RH_t)RH_m}\right)^{\frac{1}{3}} \tag{S1}$$

where $\overline{GF}_{D_0,RH,c}$ is the RH-corrected, mean, hyrgoscopic growth factor for a particle of dry diameter D_0, $\overline{GF}_{D_0,RH_m}$ is the uncorrected mean growth factor, RH_m is the measured RH and RH_t is the target RH. A full explanation of the correction applied is described by Gysel et al. (2009).

In order to propagate the error associated with the change in growth factor from this correction, Eq. S1 is differentiated with respect to RH_m to give:

$$\frac{\partial(\overline{GF}_{D_0,RH,c})}{\partial(RH_m)} = -\left((\overline{GF}_{D_0,RH_m} - 1)\frac{RH_t}{(1 - RH_t)}\frac{1}{(RH_m)^2}\right)^{-\frac{1}{3}} \tag{S2}$$

An error simulation which forms part of the TDMAinv analysis was used on the data, with the results from the error simulation showing the sensitivity of the inversion result to small changes in the measurement due to added noise (incorporating counting statistics). This helps in, for example, judging whether two peaks in the growth factor probability distribution function, $p(GF)$, can be attributed to distinct modes or whether the structure of the $p(GF)$ can be reliably attributed to distinct modes or whether they are indistinguishable from instrument noise. This is outlined in detail by Gysel et al. (2009) and is shown in Figs. 4B and C therein. 100 error simulations are performed on $p(GF)$ for each growth factor bin, and the statistical mean of these taken. The standard deviation of the mean 100 simulations was then calculated, representing the effects of counting statistics and variability in size measurement, denoted by $\sigma_{p(GF)}$. These two errors are summed in quadrature, representing the HTDMA error, GF_{error}:

$$GF_{error} = \sqrt{\left(\frac{\partial(\overline{GF}_{D_0,RH,c})}{\partial(RH_m)}0.015\right)^2 + \sigma_{p(GF)}{}^2} \tag{S3}$$

where 0.015 relates to the precision of the measurement of RH (1.5%) within the HTDMA used for the COPS experiment.

1.2 Fitting S-step and D-step CCNc data

Defined in the main text, the fitting function used for deriving the point at which $F_A(S, D_0) = 0.5$ is a sigmoidal function using orthogonal distance regression

(ODR), weighted according to the associated errors in each axis, using the Igor Pro software package and associated libraries (*ODRPACK95*, Boggs et al. 1989).

$$y = K_0 + \frac{K_1}{1 + \exp\left((x - K_2)/K_3\right)} \tag{S4}$$

Where K_0 is the base of the sigmoid (held to zero), K_1 is the maximum on the sigmoid (unconstrained to to minimise effects caused by systematic inaccuracies of either instrument), K_2 is the x value at which $y = 0.5$ (either, $D_{50,S}$ or $S_{c,D0}$, depending on the x-axis used) and K_3 is the rate.

This function is used to derive both $D_{50,S}$ and $S_{c,D0}$ for CCNc data. An example of the sigmoidal fitting to D-step and S-step interpreted data is presented in Figure S1. The fitting algorithm outputs a standard error of the x-axis value at $y = 0.5$. This is the error propagated through further calculations of quantities such as D_{thres} and N_{CCN}. S-step analysis is more sensitive to the relative positions of the data as there are only 5 data points (Fig S1a). Fitting D-step interpreted data with the sigmoidal function results in fit approaching a step function (Fig S1b).

1.3 CCNc Measurement Uncertainty

1.3.1 Uncertainty in S_{set}

In order to estimate the uncertainty in S from the standard deviation of these quantities, the standard deviation (σ) of each measurement of temperature, flow and pressure (T, Q and P respectively, which are taken to vary independently) is multiplied by its differential value, summed in quadrature and divided by the square root of the number of observations (N; number of particles measured during an averaging period) to give the standard error in S:

$$\Delta S = \frac{\sqrt{\left(\frac{\partial S}{\partial T}\sigma T\right)^2 + \left(\frac{\partial S}{\partial Q}\sigma Q\right)^2 + \left(\frac{\partial S}{\partial P}\sigma P\right)^2}}{\sqrt{N}} \tag{S5}$$

The dependence of ΔS on $\sqrt{N}$ arises because the instrument detector (the OPC) only samples the conditions when a particle is detected. As T, Q and P have been assumed to vary randomly throughout the measurement period, the more particles detected, the more precise the average supersaturation will be.

1.3.2 Uncertainty in D_0

The range of diameters introduced into the CCNc for a given target diameter is described by the DMA transfer function. For this analysis, we have assumed an ideal, triangular transfer function (Knutson and Whitby, 1975), with symmetrical bounds 5% either side of the target dry diameter, D_T. One standard deviation of this transfer function is described by $\sigma = c\sqrt{1/6}$, where $c = 0.1D_T$ i.e. the width of the base of the transfer function. When propagating the error

associated with the diameter measurement of D_T, the standard error of D_T has been used:

$$\Delta D_T = \frac{c\sqrt{(1/6)}}{\sqrt{N}} \tag{S6}$$

where N is the number of particles counted.

1.3.3 Uncertainty in number concentration

The CCNc and CPC number concentration standard errors have been calculated by invoking Poisson statistics:

$$\Delta(\sum N) = \sqrt{\frac{\sum N}{Q \sum T}} \tag{S7}$$

where N is the number of particles counted, substituted by either CCNc ($N(S, D_0)$) or CPC ($N(D_0)$), Q is the flow rate and T is the sampling time. The uncertainty in N is calculated and then propagated through the multiple charging correction procedure.

The error associated with the activated fraction, $F_A(S, D_0)$ can then be calculated:

$$\Delta(\sum F_A(S, D_0)) = \frac{N(S, D_0)}{N(D_0)} \sqrt{\left(\frac{\Delta(\sum N(S, D_0))}{N(S, D_0)}\right)^2 + \left(\frac{\Delta(\sum N(D_0))}{N(D_0)}\right)^2} \tag{S8}$$

References

[Boggs et al. (1989)] Boggs, P., Donaldson, J., Byrd, R., and Schnabel, R.: Algorithm 676: ODRPACK: software for weighted orthogonal distance regression, ACM Transactions on Mathematical Software (TOMS), 15, 364, 1989.

[Gysel et al. (2009)] Gysel, M., McFiggans, G., and Coe, H.: Inversion of tandem differential mobility analyser (TDMA) measurements, Journal of aerosol science, 40, 134–151, 2009.

[Knutson and Whitby (1975)] Knutson, E. and Whitby, K.: Aerosol classification by electric mobility: apparatus, theory, and applications, Journal of Aerosol Science, 6, 443–451, 1975.

[Rose et al. (2008)] Rose, D., Gunthe, S., Mikhailov, E., Frank, G., and Dusek, U.: Calibration and measurement uncertainties of a continuous-flow cloud condensation nuclei counter (DMT-CCNC): CCN activation of ammonium sulphate and sodium chloride particles in theory and experiment, Atmos. Chem. Phys, 8, 1153–1179, 2008.

2 Supplementary Figures
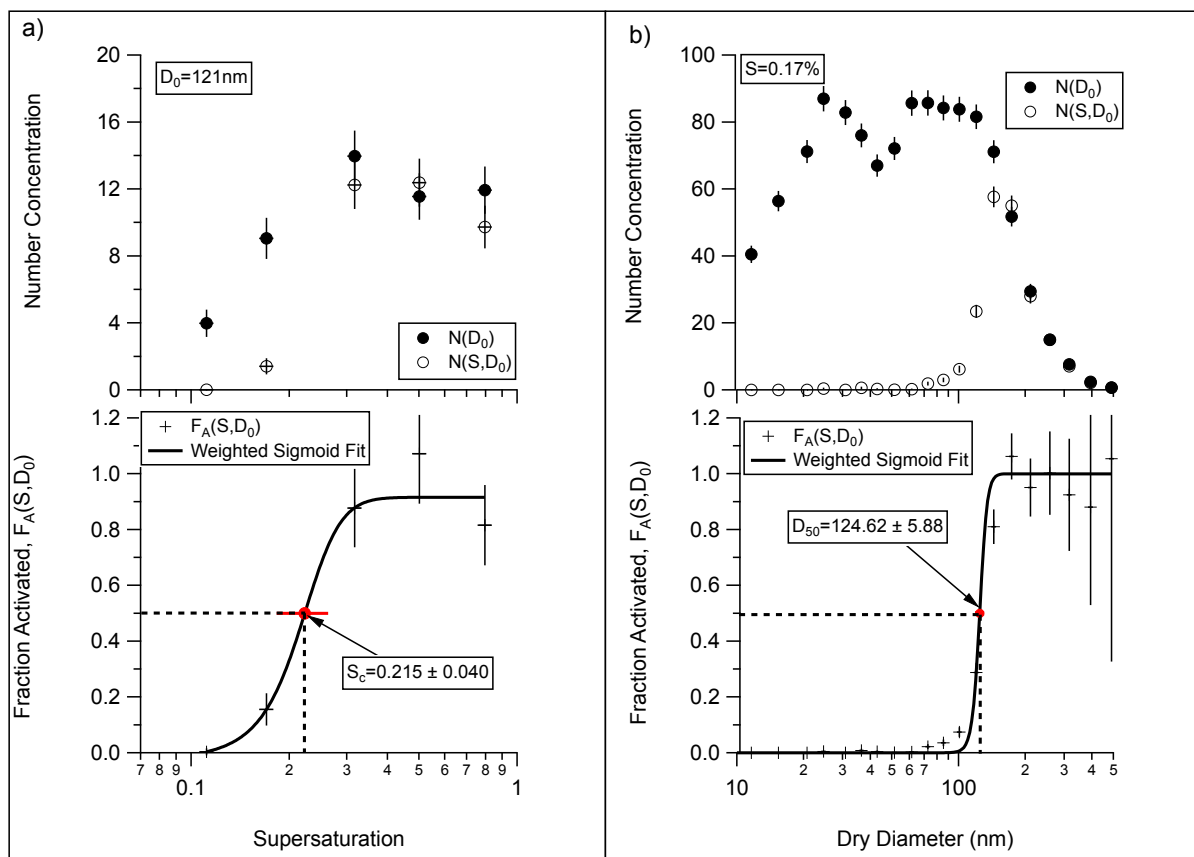
Figure S1: a) S-step interpreted data for $D_0 = 121$ nm, showing the relative number concentrations from CCNc and CPC, with their respective uncertainties in the top panel, and the bottom panel showing the sigmoid fit to $F_A(S, D_0)$ vs S_{set}. b) D-step interpreted data for the supersaturation setting 0.17%, illustrating the almost step-function sigmoidal fit to the D-step analysis, and subsequently reduced uncertainty.
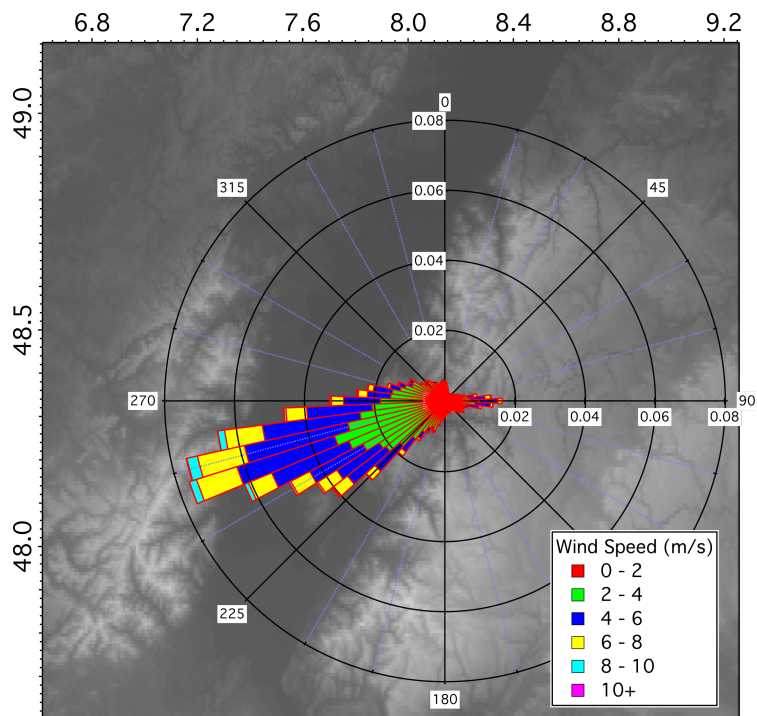
Figure S2: Wind rose centred on measurement location. The prevailing wind passing up the Rhine valley into the COPS region at around 5m/s average wind speed (measured at 1166m ABSL, 2m AGL).
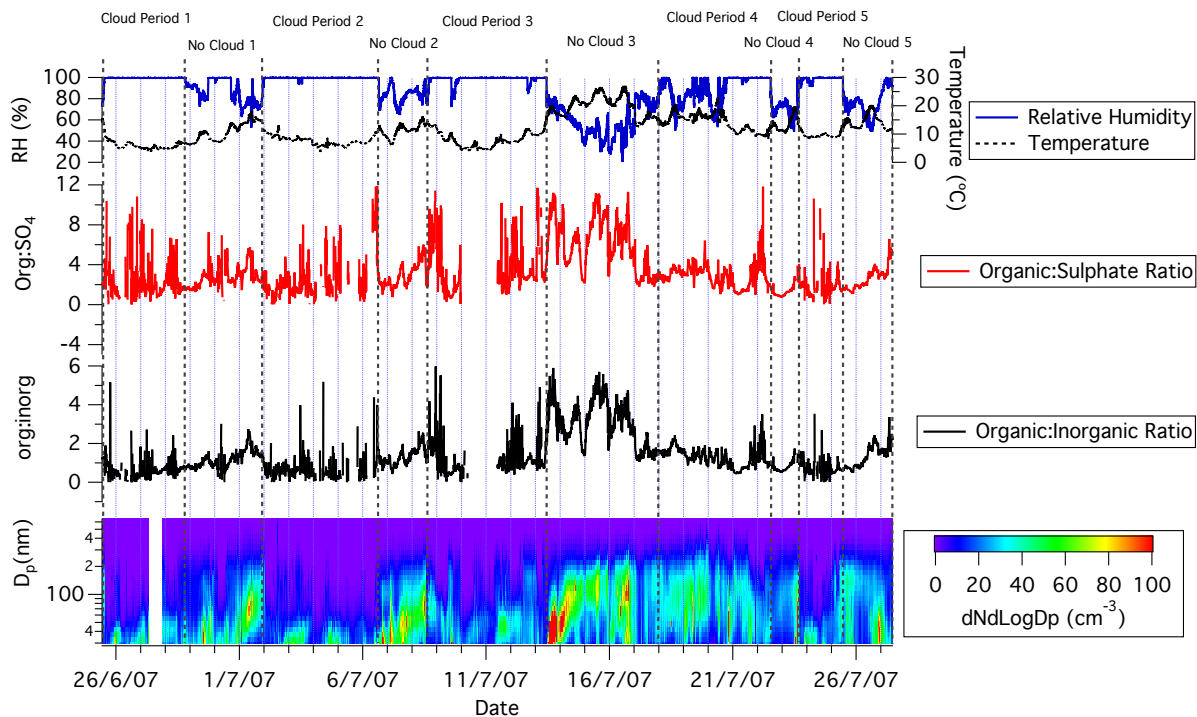
Figure S3: Relative Humidity (RH), organic:sulphate ratio, organic:inorganic ratio and $dNdlogDp$ for the measurement period, segregated into "cloud periods" and "no cloud" periods. Cloud periods are defined by $RH \geq 85\%$ and are characterised by a low organic:inorganic ratio and typically relatively low number concentrations ($D_0 < 600$ nm). 'No cloud' periods are characterised by higher a organic:sulphate ratio and tend to start with high concentrations of small (≤ 40nm particles, which grows into a large (≈ 150nm), strongly monomodal size distribution.
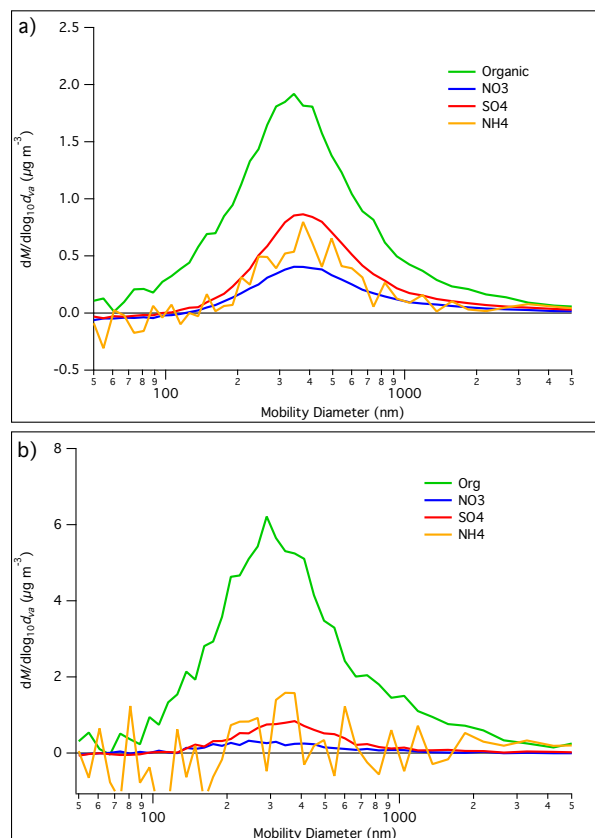
Figure S4: Size resolved AMS data for both a) $\leq$ 4:1 and b) $\geq$ 4:1 organic:sulphate ratio periods. The high organic to sulphate ratio periods (b) show a dramatic relative increase in organics above 100nm, with the majority of the organic fraction around 300nm.
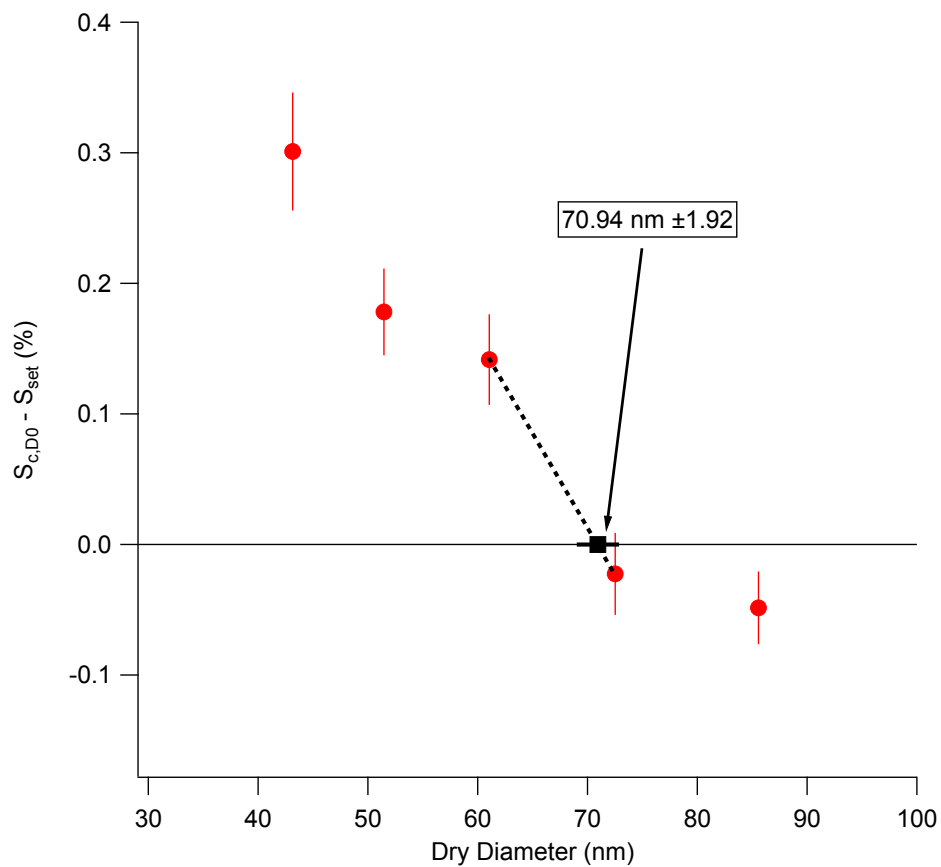
Figure S5: A graph showing $S_{c,D_0} - S_{set}$ vs D_0. The two data points straddling the zero line are linearly interpolated between, with the intercept defining the physical threshold diameter of the aerosol, $D_{thres,Sc}$. The errors on $D_{thres,Sc}$ are propagated using standard procedure.
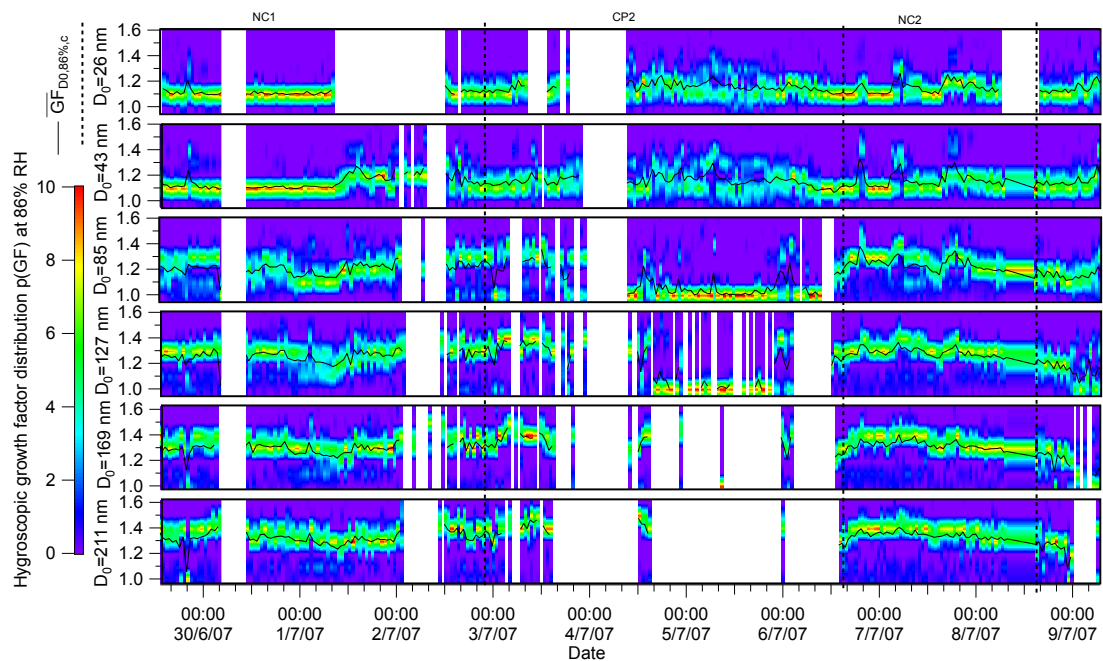
Figure S6: A reproduction of Figure 1, focussed on NC1 through NC2, showing measured HTDMA hygroscopic growth factor probability distribution, $p(GF)$, as a function of time. It can be seen that the HTDMA growth factor distribution is typically well represented by the mean growth factor, $GF_{D0,86\%,c}$, though there is an increasing prominence of bimodality seen with an increase of size.